JOINT EUROPEAN TORUS

JET–P(90)31

M.G.von Hellermann, W. Mandl, H.P. Summers, H. Weisen, A. Boileau, P.D. Morgan, H. Morsi, R. Koenig, M.F. Stamp, R. Wolf and JET Team

Visible Charge Exchange Spectroscopy at JET

Visible Charge Exchange Spectroscopy at JET

M.G.von Hellermann, W. Mandl, H.P. Summers, H. Weisen[1], A. Boileau[2], P.D. Morgan, H. Morsi, R. Koenig, M.F. Stamp, R. Wolf and JET Team*

JET-Joint Undertaking, Culham Science Centre, OX14 3DB, Abingdon, UK

[1]CRPP, Avenue des Bains, Lausanne, Switzerland
[2]CCFM Tokamak de Varennes, Canada
** See Appendix 1*

Preprint of Paper to be submitted for publication in
Review of Scientific Instruments

ABSTRACT.

Recent developments and results of the JET CXRS diagnostic are reported. The measurement of radial profiles of ion temperatures and densities are based on CXR spectra of fully-stripped ions of either carbon or beryllium. Considerable effort has been expended in ensuring consistency between radial profiles of low-Z impurity densities and those from other diagnostics. The contributions of the main light impurities are used to reconstruct radial profiles of Z_{eff} which can be compared with Abel-inverted signals from visible bremsstrahlung or soft x-ray emission.

Active Balmer-Alpha spectroscopy (ABAS) is being introduced as a diagnostic tool providing data on local magnetic fields, neutral beam densities and dilution factors.

The effects of collision-energy-dependent CXR cross-sections on observed CXR spectra are calculated. Corrections for the values of deduced ion temperatures, toroidal velocities and impurity densities are discussed for the case of plasmas with high ion temperatures and high toroidal rotation velocities·.

Some recent results of the JET 1989 operation illustrating the CXRS diagnostic potential are given.

Introduction

Charge Exchange Recombination Spectroscopy (CXRS) is used at the JET tokamak for the deduction of radial profiles of ion temperature[1,2], plasma rotation[3] and low-Z impurity densities[4,5,6,7]. Deuteron concentrations[8,9] are derived from the simultaneous density measurement of the main low-Z impurities, carbon and oxygen (or beryllium), and that of the electrons.

More recently, the introduction of Active Balmer-Alpha Spectroscopy (ABAS)[9,10], which makes use of line emission spectra from fast injected neutrals and that from CX spectra of thermal deuterons, has provided a further diagnostic tool enabling a self consistent deduction of local impurity concentrations. Radial profiles of the effective ion charge Z_{eff} can be derived from line intensity ratios in the active Balmer-Alpha spectrum without the need of absolute calibration and only a weak dependence on electron density data. An absolutely calibrated system allows direct measurement of local deuteron concentration and neutral beam density.

The wavelength separation in the motional Stark multiplet[10] and its polarisation pattern[11,12] can be used to derive the local magnetic field strength and the orientation of the field vector. Results at JET have shown that values of local field strength can be derived with accuracies of a few percent. Presently a system measuring both orientation and total field strength is being prepared.

An intensive effort has been put into the maintenance and enhancement of the JET atomic data base[13] . The effective emission rates following charge capture and n- and l-redistribution processes are modelled to the plasma environment, that is to the values of beam energy, ion temperature and ion and electron density.

The effective CX cross sections may change significantly over the thermal velocity range in the case of high ion temperature plasmas usually with strong toroidal rotation and highly peaked ion temperature profiles. The velocity dependence of the effective emission cross section results in a distortion of the observed spectrum, which deviates from the original Maxwellian velocity distributin function. The observed spectrum may have an apparent Doppler-shift, for example due to an enhanced cross-section for the particles moving in the direction of the neutral beam, and a reduced cross-section for particles moving in the opposite direction. The actual Doppler-width may consequently be reduced and lead to an apparently reduced temperature value. We have investigated in great detail similar effects on CX spectra expected from slowing-down and thermalized alpha particles[14,15], and the detection limit of helium minority densities using present (80 keV) and future JET heating beams (160keV) .

Instrumentation and Data Analysis

The analysis procedure for CXRS data (see Fig. 1) and the layout of viewing lines and instrumentation has been described in earlier papers[1,2,4,5]. Two instruments collecting the light from a single vertical channel which intersects the neutral beams in the plasma centre are dedicated to the main light impurities (C and Be) . A fan of 12 horizontal lines of sight in the toroidal mid-plane is used for the profile measurements. The light from all channels is recorded simultaneously by a 2-dimensional instrument tuned to the impurity lines of C or Be and D, respectively.

For the next operation period of JET two 2-dim instruments will be used at the same time, one being constantly dedicated to the analysis of the deuterium Balmer-alpha spectrum. A polarising beam splitter arrangement will be implemented in the near future for the measurement of both the wavelength splitting and the polarisation pattern in the neutral Balmer-Alpha emission spectrum. This will enable the deduction of magnetic field strength and its orientation.

A new fibre-less UV optical link (200nm to 700nm) between torus hall and two further remote instruments is presently commissioned. This system gives access to further CXRS lines below 400nm (for example the CX He^{+} 5 to 3 transition at 3200 Å). A much enhanced optical throughput will allow a temporal resolution with sampling rates of the order 1 kHz.

In addition to the CXRS lines of sight we make use of the viewing lines dedicated to passive emission spectroscopy in the visible wavelength range[16]. Bremsstrahlung radiation and some dedicated impurity lines are recorded by several lines of sight directed onto the limiters, walls and horizontal midplane. A poloidal fan of 15 lines-of-sight is used for the analysis of visible bremsstrahlung, and subsequent Abel inversion provides Z_{eff} profiles.

Calibration and Consistency Checks

The deduction of impurity densities is based on absolute calibration of all instruments and - during JET operation - on additional consistency checks with bremsstrahlung measurements and neutral beam D-α emission spectra (see active Balmer-alpha spectroscopy).

The absolute sensitivity of the single point system is monitored continously by comparison of the Bremsstrahlung level with that of similar lines of sight. A survey over a long operation campaign showed that the various vertical lines of sight at JET with top windows[4,16] far away from the plasma agreed within 20% and that cross calibration factors were stable in time.

The bremsstrahlung measurement by the CXRS multi-chord system with its fan of viewing lines in the equatorial midplane, is more difficult for two reasons. The collecting mirror and vacuum window close to the plasma boundary have a continously-decreasing transmission in the course of an operational campaign. An attempt to monitor the actual transmission by measuring the continuum radiation level showed - in particular in the case of low-density plasmas and low values of Z_{eff} - that the signal levels are comparable to the electronic dark current of the vidicon detector system.

We use therefore as a rule the CXRS density results from the single vertical channel, representing the plasma centre, to cross-calibrate the profiles of the multi-chord system.

In order to compare resulting profiles of low-Z impurities with those deduced from visible bremsstrahlung we use a quantity, equivalent to the line-averaged bremsstrahlung signal,

$$<Z_{eff,CXRS}> = \int dr \; Z_{eff}(r) \; w(r) \; / \int dr \; w(r)$$

with $w(r) = n_e^2(r)/\sqrt{T_e(r)}$

$$Z_{eff}(r) = 1 + \sum Z(Z\text{-}1) \; n_Z(r)/n_e(r)$$

The ratio of $Z_{eff}(r{=}0)/ <Z_{eff,CXRS}>$ is a measure of the hollow or peakedness of a radial profile. Statistical surveys have for example shown that in the 1989 berylllium belt-limiter phase Z_{eff} profiles tend to be slightly peaked, in contrast to the X-point configuration with typically hollow concentration profiles[6]. This may be due to much enhanced gas fuelling and pumping in the belt-limiter configuration, whereas in the X-point configuration an enhanced impurity influx from the target plate is observed.

Neutral Beam Penetration

The neutral beam penetration is calculated in two steps. In a first step a line averaged value of Z_{eff} and a constant ratio of the main impurities is used to derive the concentrations of impurities contributing to the beam attenuation. The densities calculated from the intensities of the two central CX spectra provide values of the actual impurity mixture (for example the density ratio carbon:oxygen or carbon:beryllium). In a second iteration, the time evolution of the concentrations of the two main impurities is used in the beam penetration code. The beam penetration is only to zero order approximation independent of the impurity contributions, but may be a sensitive function of the impurity mixture at high values of Z_{eff} , due to the fact the cross-sections involved depend non-linearily on Z (cf. Ref.4). It is, however, assumed that the ratio of impurities is a constant over the radius.

Error analysis

In principle, all the spectroscopic measurements aim ultimately to establish a profile of the deuteron concentration. The overall error for absolute impurity densities as a result of uncertainties in absolute calibration, electron density, beam geometry and atomic data on cross-sections is estimated to be 30 to 40% for carbon, oxygen or beryllium. The error in dilution factor n_d/n_e = $1 - \sum_k Z_k\, n_Z/n_e$ does strongly depend on the level of n_d/n_e itself. In fact in pure plasmas ($Z_{eff} < 2$) it is more sensible to accept the uncertainties in CXR cross sections for carbon and beryllium and derive from their densities the deuteron concentration, than using the CXR analysis of thermal CXR spectra of deuterium. The relative error for the dilution factor $d = n_d/n_e$ can be expressed as:

$$\frac{\delta d}{d} = \frac{1 - d}{d} \frac{\delta c}{c}$$

Assuming for example a 30% error in impurity concentration $c = n_Z/n_e$ we obtain at a dilution level of 0.8 a relative error of only 7%. By the same argument at a level of d = 0.5 the relative error will be 30%.

Effects of cross-sections in hot fusion plasmas on CXRS analysis

In high temperature or rapidly-rotating plasmas the observed CX spectrum will be affected by a varying effective charge capture cross-section. This is caused either by the spread of thermal velocities of particles contributing to the spectrum, which averages over the collision-energy -dependent cross-section, or by a shift in relative velocity between bulk plasma and neutral beam due to high rotation velocities. Obviously, the higher the velocity of the thermal plasma particles - in particular for low mass ions such as deuterons and helium ions - the bigger the effect.

As a result of this effect, apparent temperatures and rotation velocities may be derived from observed CX spectra. Significantly-changed values of effective charge capture cross-sections are possibly even more important. The latter may affect the value of deduced impurity densities as well as calculations for beam penetration.

The implications for the analysis of fusion plasmas were already recognized in earlier works[17,18,19] . The predictions of the observed spectral profiles depend sensitively on the precise shape (that is absolute level and gradient) of the emission cross-sections as a function of collision energy. JET has initated a comprehensive programme to establish theoretical as well as experimental data[20,21,15,22] for the analysis of low-Z impurities and in particular for alpha particles (based on visible CXRS). In this paper we present some of the results calculated for the effects on thermal spectra of He^{+}(4 to 3) and C^{5+} (8 to 7). A detailed paper on the feasibility of alpha-particle detection at the JET tokamak is presently prepared.

Fig.2 gives some results for the deduction of temperature, velocity and density for C^{6+} (Fig. 2a,b,d) and He^{2+} (Fig. 2c), calculated for a beam energy of 40 keV/amu and a non-rotating plasma.

For C^{6+}(at 5290.5 Å) the maximum deviation from the true temperature is less than 8% (2keV), even in the case of central ion temperatures of 30 keV. The differences between apparent and true temperatures are much stronger in the case for the He transition (Fig.2c , $\Delta T = 6$ keV at $T = 30$ keV).

The quoted apparent velocities in Fig.2b refer to Doppler-shifts in observation direction. The corresponding values in toroidal direction are derived from the angles between viewing line and magnetic flux surface. The central viewing line of the JET CXRS diagnostic intersects the neutral beams at an angle of $120^{\circ}$and is tangential to the magnetic flux surface. The outermost line of sight has an intersection angle of 150° . Since the apparent velocity effect depends both on intersection angle and local temperature we have a compensation of low-temperature and large-angle effects at the boundary and high-temperature and smaller angle in the plasma centre.

The changes of effective rate coefficients as a function of ion temperature are shown in Fig. 2d, for the central l.o.s. with different toroidal velocities as parameter.

Active Balmer Alpha Spectroscopy

Fast injected neutral deuterium atoms from the heating beams experience collisions with plasma ions (deuterons and impurities) and emit light at the Balmer-alpha wavelength. In the energy range of 40 keV/amu, impact excitation by electrons is less significant but needs to be taken into account for the fractional energy species. Active Balmer-alpha spectroscopy (ABAS) makes use of both the line radiation from the CX reaction with plasma deuterons *I(CX)*) and the relaxation radiation from excited fast deuterium atoms in the neutral heating beams *I(b)* . Fig. 3 shows the two very intense, well separated spectral features. The Doppler-shifted part representing the fast neutrals shows a multiplet structure due to the motional Stark effect ($\mathbf{E}_{\mathbf{Lorentz}} = \mathbf{v}_{\mathbf{beam}} \times \mathbf{B}$). Details of this spectrum are described in[10].

For the analysis of impurity densities we discuss in this paper the use of simultaneous I(CX) and I(b) measurements.

$I(CX) = n(D) \sum_E n_b(E)\ q_{CX}(E,n=3,n=2)$

with $n(D)$ deuteron density, $n_b(E)$ fractional beam density and q_{CX} effective CX rate

$I(b)=\sum_E \sum_Z n_b(E)\ n(Z)\ q_{impact}(Z,E,n_e)$ with $n(Z)$ ion density (including impurities and deuterons), $q(Z,E,n_e)$ effective impact excitation rate for impurities and electrons, indices E and Z refer to summation over all beam energy species and impurities.

The effective emisssion cross-sections and their dependencies on ion charge, beam energy and electron density have been recently updated in the JET atomic data base. We show here some of the results (Fig.4) and refer to more comprehensive presentations in a later paper .

For an absolutely calibrated system, the local neutral-particle density can thus be determined directly from the line intensities I(b) and can be used as a cross reference for the low-Z impurity analysis. Vice versa, if we accept the neutral beam density as derived from an electron density profile and beam stopping cross sections, we may use the comparison as a measure of the actual absolute sensitivity of each multi-chord channel. We have used this technique for a cross-check of relative sensitivity .

As illustrated in Fig. 5, the relative intensity of the impact spectrum I(b) compared with the intensity of the CX spectrum I(CX) is a sensitive function of the local value of Z_{eff} . In principle, the ratio can therefore be used to determine radial Z_{eff} profiles without the need of absolute calibration, electron density data, or any Abel-inversion. A detailed analysis is presently being prepared. The actual problem is the unambiguous separation of the Doppler broadened features in the unshifted Balmer-Alpha spectrum. The 'pedestal' indicated in Fig. 3., representing a CX excited emission layer near the plasma edge, requires specific attention in the ABAS fit.

Recent Results

1)Ion Temperatures

Generally, the different ion temperature diagnostics at JET agree within 10 to 20% and give reliable values for the central ion temperatures[2,4]. Radial profiles, however, are only provided by the CXRS diagnostic with its 12 radial channels. Fig.6 shows an example of central ion temperatures measured during ohmic and combined additional heating phases. The CX temperature is based on the Be IV(6 to 5) transition. The ion temperatures derived from calibrated neutron yield are only calculated in the ohmic heating phase where thermal neutron production and Maxwellian distribution functions can be expected. No systematic differences were found in ion temperatures based on either beryllium or carbon.

In Fig. 7 we show examples of ion temperature profiles obtained in double null X-point configuration with different heating powers ranging from 1.2 to 18 MW. The ratio of central to volume-averaged temperature $T_i(0)/\langle T_i \rangle$ is found to increase almost linearily with central temperature during a NB heated pulse and may reach values up to 5 in low-density high-ion-temperature plasmas (n_e=4 $10^{19}m^{-3}$, $T_i(0)$ = 25 keV). In two of the profiles shown (b and c) the plasma was radially swept at a rate of 1 Hz and amplitudes between 6 and 12 cm, providing a continuous coverage of the profiles during stationary phases of the discharge. For this reason, we show the profiles as a function of the distance to the last closed flux surface (LCFS) obtained from magnetic probe measurements. The plasma centre corresponds to a distance of approximately 1m. The profile d) in Fig. 7 was obtained less than 50 ms after the beginning of NBI, and can be taken to be representative of ohmic conditions.

Another feature of interest is the high edge ion temperatures shown in the figure. A measurement at the LCFS was obtained in the experiments shown in Fig. 7b and 7c where the LCFS was swept accross our outermost viewing volume, located at a major radius of 4 m. As the viewing volume came to lie outside the LCFS, our charge exchange signals dropped to a few percent of those from the neighbouring volume, which was entirely within the LCFS, leaving only a background line with a temperature somewhat higher than obtained at the LCFS. It corresponds to the so-called 'cold component' (cf. Ref.4) , from C^{+5} near the edge, and which is also observed without neutral beam heating. The 'cold' temperature is approx. 800 eV with ohmic heating alone, and can be up to 3 keV in high power H-modes (Fig.7b). It matches the plasma ion temperature at a location about 10 to 20 cm inside the LCFS (Fig.7), indicating its approximate radius of the emission shell.

Remarkably, the ion temperature gradients remain constant throughout the outer 30 to 50 cm of the discharge, right up to the LCFS, where ion temperatures exceed the electron temperature by an order of magnitude . Such high edge ion temperatures are necessary to explain the heat flux to the limiting surfaces obtained from Langmuir probe measurements[23]. With our present spatial resolution we cannot identify any region near the LCFS, where ion temperatures decrease to values comparable to electron temperatures measured using Langmuir probes (~ 40 eV). Should such a region exist just inside the LCFS, it would have to be less than about 3cm in radial extend to be masked by the 'cold' component and escape detection in the radial sweep experiments. Clearly, the resolution of edge ion temperature and ion density measurements needs to be improved. They have important implications for the understanding of heat deposition and impurity production at the plasma-vessel interface, as well as for the particle transport into the discharge.

In most NB-heated discharges the toroidal angular momentum is proportional to the ion temperature throughout the entire profile, $\omega \cong 8 \text{ rad s}^{-1}\, T_i$, independently of the plasma conditions, as shown in Fig. 8. Since beam energy and momentum deposition profiles are proportional to each other, this implies that ion heat and momentum diffusivities are also proportional to each other. The proportionality factor has been found to be close to 1 in a pure hydrogen plasma [24].

Exceptions arise in the presence of strong MHD or strong RF heating, where the toroidal rotation falls below the values given by the above scaling. In the case of strong MHD activity, the additional momentum losses appear to be absorbed by electromagnetic interactions of the modes with the vessel walls[3]. Least understood is the effect of RF heating on plasma rotation. In some cases of combined RF/NB heating with $P_{RF} \gg P_{NB}$, the RF has been observed to drive plasma rotation in the direction opposite to that of the beams.

2) Impurity Behaviour and Plasma Purity

In an effort to decrease plasma contamination by impurities, the JET 1989 programme was primarily devoted to assessing the properties of beryllium as a limiting material. In a first step, beryllium was evaporated onto the vessel walls to evaluate its gettering and pumping effects. At the end of the campaign the power handling capabilities of a pair of bulk beryllium belt limiters were assessed. The dramatic improvements in target plasma purity and performance of additionally-heated discharges can mainly be attributed to oxygen removal and improved density control resulting from the gettering action. In many conditions, however, the performance of high power heated discharges was still limited by the appearance of hot spots on the limiting surfaces, where substantial sublimation or melting occured, releasing large amounts of impurities.

An overview of improvements in central deuterium dilution n_d/n_e of neutral beam heated discharges is shown in Fig. 9 for the different phases. The total of all observations during the heating pulses are represented here and no particular time slices were selected. The dilution factor was obtained by adding the contributions of carbon and beryllium, which were measured simultaneously at the plasma centre.

The improvement of the quality of target plasmas for heating experiments was particularly dramatic, with $Z_{eff}(0)$ decreasing from typically 4 without beryllium to about 1.5. Be-concentrations measured by CXS dropped from about 2% to below 0.5% within the first four additionally heated discharges after evaporations. The carbon concentrations of the target plasmas (≤2%) remained virtually unaffected. This behaviour is interpreted as being due to the burning out of the beryllium layer, about 0.2μm thick..

The improved plasma purity, together with the better density control due to the strong pumping by the beryllium covered surfaces, led to a substantially enhanced plasma performance, as in Fig. 10a, which shows an X-point plasma with up to 17 MW of NBI which attained an ion temperature of 22 keV and and a fusion product $n_d\ T_i\ \tau$ of $9\times10^{20}m^{-3}$keV s in the plasma centre.

Following formation of the X-point configuration after t=8 s, the central beryllium concentration dropped steadily from an initial 3.5% to about 1%, while the central carbon concentration first increased from 0.3% to 3% at 9.5 s, before being diluted down again to 1% at 11.4 s by NB fuelling (Fig.10d). Fig. 10c shows that the central Z_{eff} obtained by adding the contributions of carbon and beryllium, are in good agreement with the line averaged value from visible Bremsstrahlung. Also shown in Fig. 10d is the carbon concentration at R=3.8m. Carbon concentration profiles remained fairly flat until 0.5 s after application of the full NBI power, when a carbon influx was first detected at the outermost CXS viewing positions, producing a hollow profile. The influx became catastrophic at 11.5 s, terminating the high fusion performance.

Conclusions

The combination of simultaneous measurements of the main impurities, visible bremsstrahlung and light emitted by neutral beam atoms enables a consistent description of radial impurity profiles. In spite of remaining uncertainties in absolute sensitivity, observation geometry, neutral beam density and atomic data on cross sections, developments in the present CXRS analysis have clearly turned the diagnostic into a very powerful and versatile tool. The recent change in the JET tokamak to beryllium as limiter material has enforced new approaches to absolute calibration during extended operation period because access to contaminated windows is restricted. Active Balmer-Alpha spectroscopy may turn out in future to be a useful tool for absolute calibration and self-consistent impurity analysis.

Acknowledgement

The authors are greatly indebted to Drs Wolfgang Engelhardt and Paul Thomas who have continously encouraged and stimulated the development of the CXRS diagnostic at JET. The entire JET team is acknowledged in its contribution to numerous data and discussions.

References

[a]CRPP, Ave des Bains, Lausanne, CH, [b]CCFM Tokamak de Varennes, Canada

[1]H Weisen, M von Hellermann, A Boileau et al. Nucl. Fusion **29**, 2187(1989)

[2]H.Morsi, M von Hellermann, R.Barnsley et al., 17th EPS, Amsterdam (1990)

[3]J.Snipes, D.J.Campbell, T.C.Hender et al. Nucl.Fusion **30**,205(1990)

[4]A.Boileau, M von Hellermann,L.Horton et al. Pl.Ph.Contr.Fus.**31**,779(1989)

[5]A.Boileau, M von Hellermann, L.Horton et al. Nucl.Fus.**29**,1449(1989),

[6]M von Hellermann, A.Boileau, W.Mandl et al, 31st APS(1989), Anaheim, Cal.

[7]H.Weisen, M von Hellermann, D.Pasini et al. Proc., EPS Amsterdam(1990)

[8]N.Jarvis, J.M.Adams, B.Balet et al., Nuclear Fusion, **30**,307(1990)

[9]A.Boileau, M. von Hellermann, W.Mandl et al. J.Phys.B,**22**, L145(1989)

[10]W.Mandl, M von Hellermann, P.Morgan et al., Proc EPS Amsterdam (1990)

[11]D.Wroblewski, K.H.Burell, R.Seraydarian et al., 31st. APS(1989),Anaheim

[12]F.Levinton, R.J. Fonck, G.M.Gammel et al. ,Phys. Rev. Lett.

[13]H.P.Summers, R.Gianella, M von Hellermann et al., 'JET Spectra and their Interpretation', in 'Atomic Spectra and Oscillator Strength for Astrophysics and Fusion', to be published by North Holland Publ.(1990)

[14]M von Hellermann, H.P.Summers, A.Boileau, 15thEPS, Dubrovnik 1988

[15]J.Frieling, R.Hoekstra, F.J.de Heer et al., 17th EPS, Amsterdam(1990)

[16]P.D.Morgan, K.H.Behringer, P.G.Carolan et al. Rev.Sci.Instr.**56**,862(1984)

[17]N.Gowern, B.Core , JET Report JET-DN-T(84)42, JET 1984

[18]M von Hellermann et al., IEA Large Tokamak Workshop on Ion Temperature Measurements, PPL Princeton N.J. , Nov. 1987

[19]R.B.Howell, R.J.Fonck, R.J.Knize, K.P.Jaehnig, Rev.Sci.Ins.**59,**1521(1988)

[20]W.Fritsch, Phys Rev.**A38,**2664(1988)

[21]W.Fritsch, J.Phys.Coll. **50**,87(1989)

[22]R.Hoekstra, Thesis(1990), Rijksuniversiteit Groningen, The Netherlands

[23]S K Erents et al, 17 th EPS, Amsterdam, 25-29 June 1990

[24]H P L de Esch, D Stork, H Weisen, 17 th EPS, Amsterdam, 25-29 June 1990

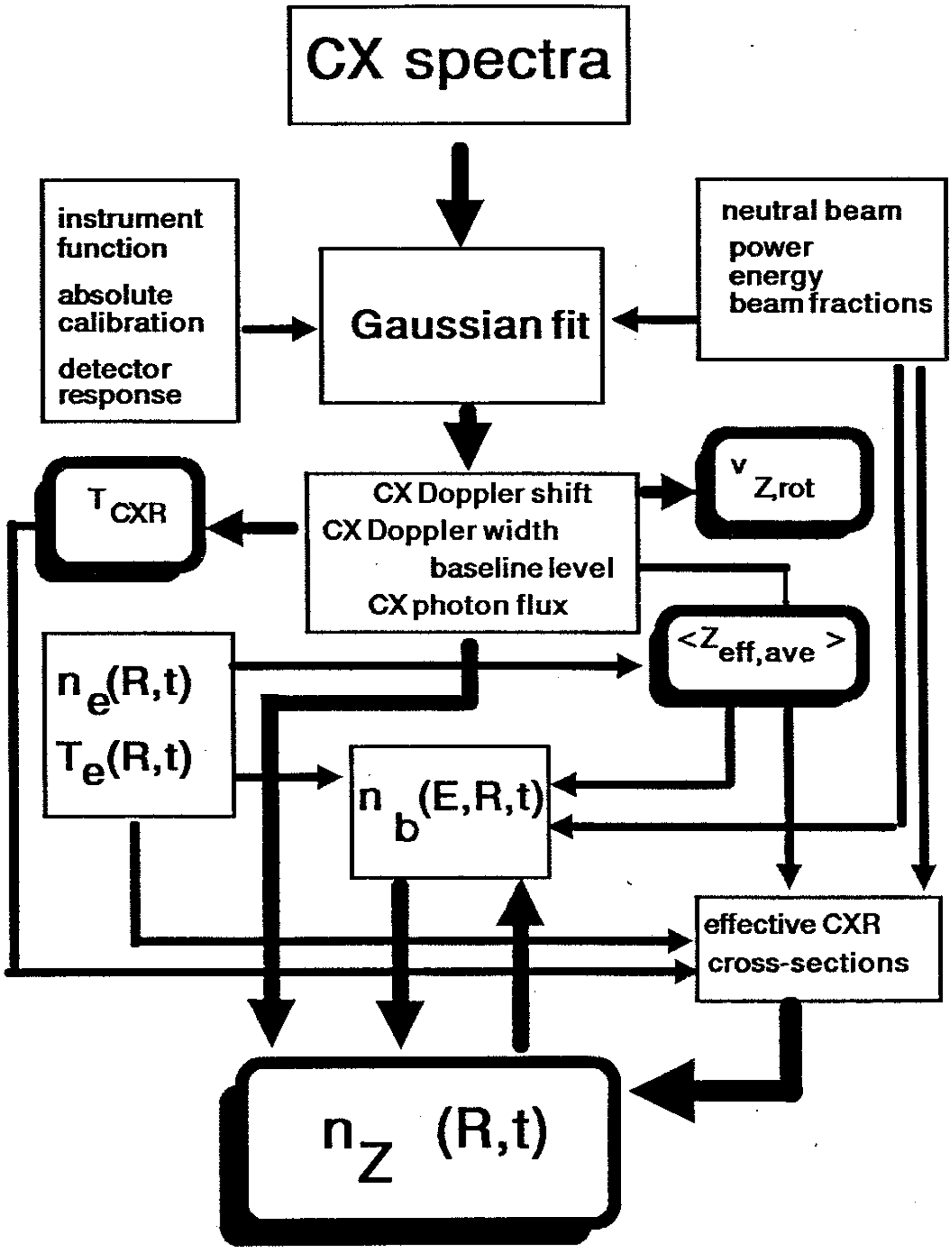

Fig.1 Flow-chart of CXRS analysis at JET

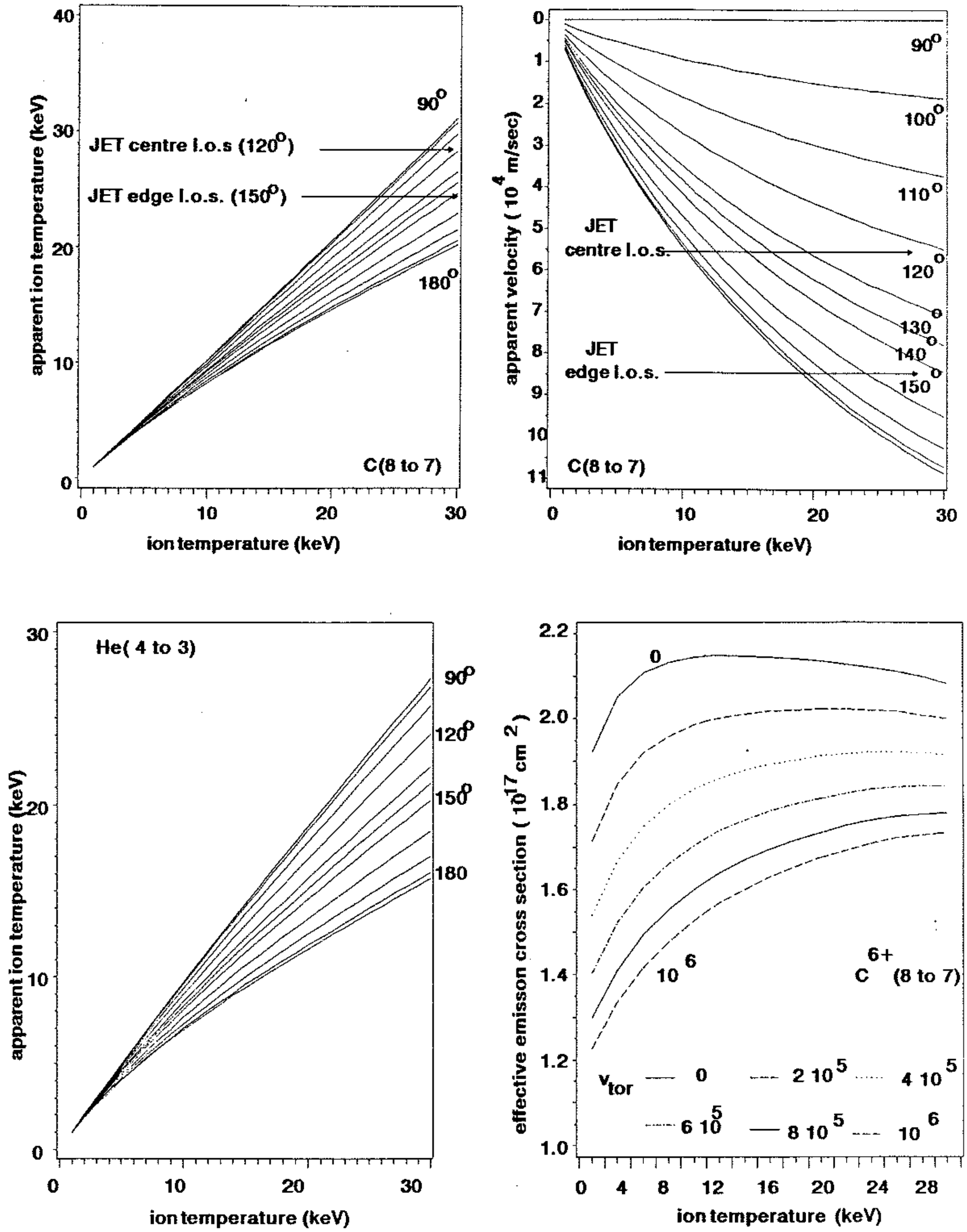

Fig.2 Effects of collision energy dependent CX (C^{5+},n=8 to n=7) cross-sections for a beam energy of 40keV/amu on a) apparent temperature, b) apparent velocity (in observation direction), c) apparent temperature in the case of He (n=4 to n =3). The parameter is the angle between neutral beam and line of sight. In the JET CXRS geometry 120^0 corresponds to the plasma centre and is tangential to the magnetic flux surface; d) effective emission cross section of the CX C^{5+}(n=8) transition in the case of the central l.o.s. for toroidal rotation velocities between 0 and 10^6 m/sec.

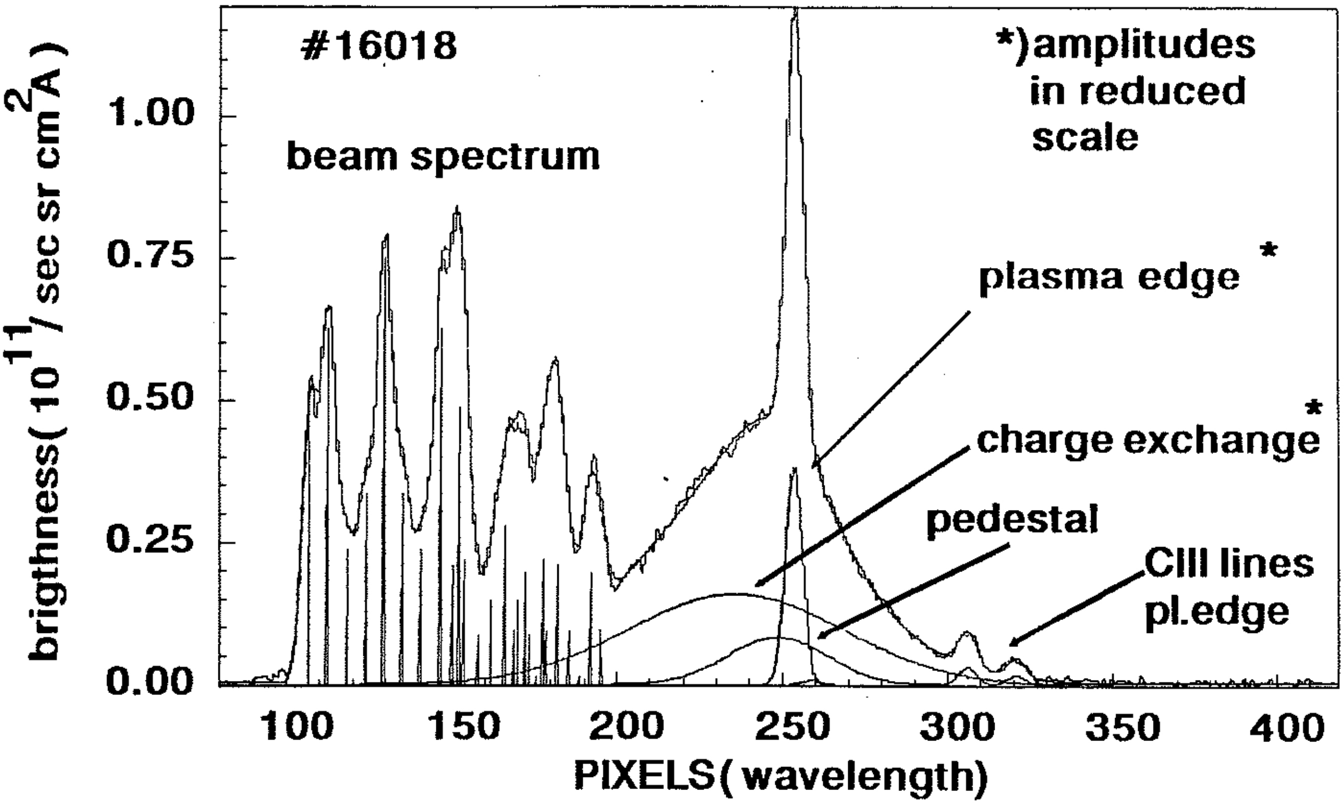

#16018
*)amplitudes in reduced scale
beam spectrum
plasma edge *
charge exchange *
pedestal
CIII lines pl.edge
brightness(10^{11}/ sec sr cm^2A)
1.00
0.75
0.50
0.25
0.00
100
150
200
250
300
350
400
PIXELS(wavelength)

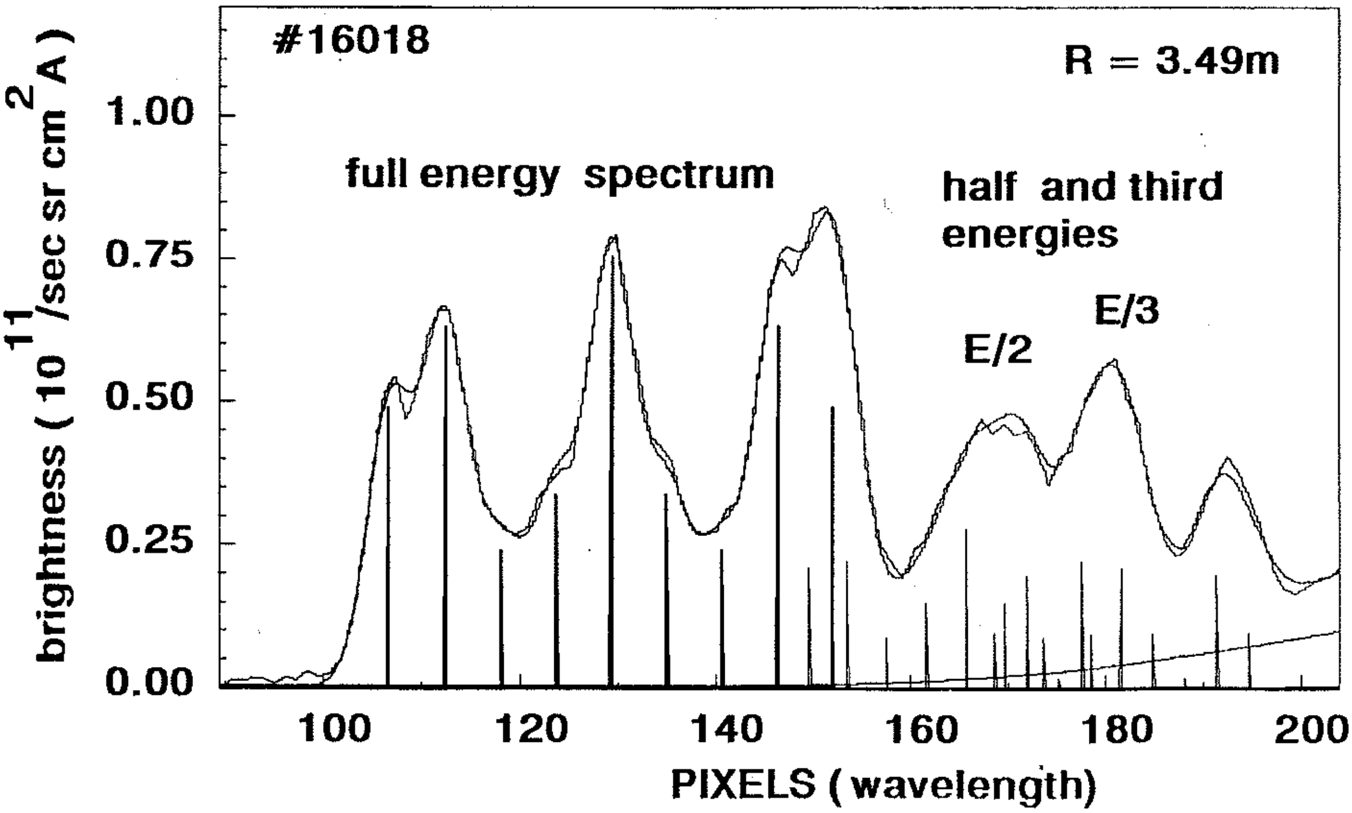

#16018
R = 3.49m
full energy spectrum
half and third energies
E/2
E/3
brightness (10^{11}/sec sr cm^2A)
1.00
0.75
0.50
0.25
0.00
100
120
140
160
180
200
PIXELS (wavelength)

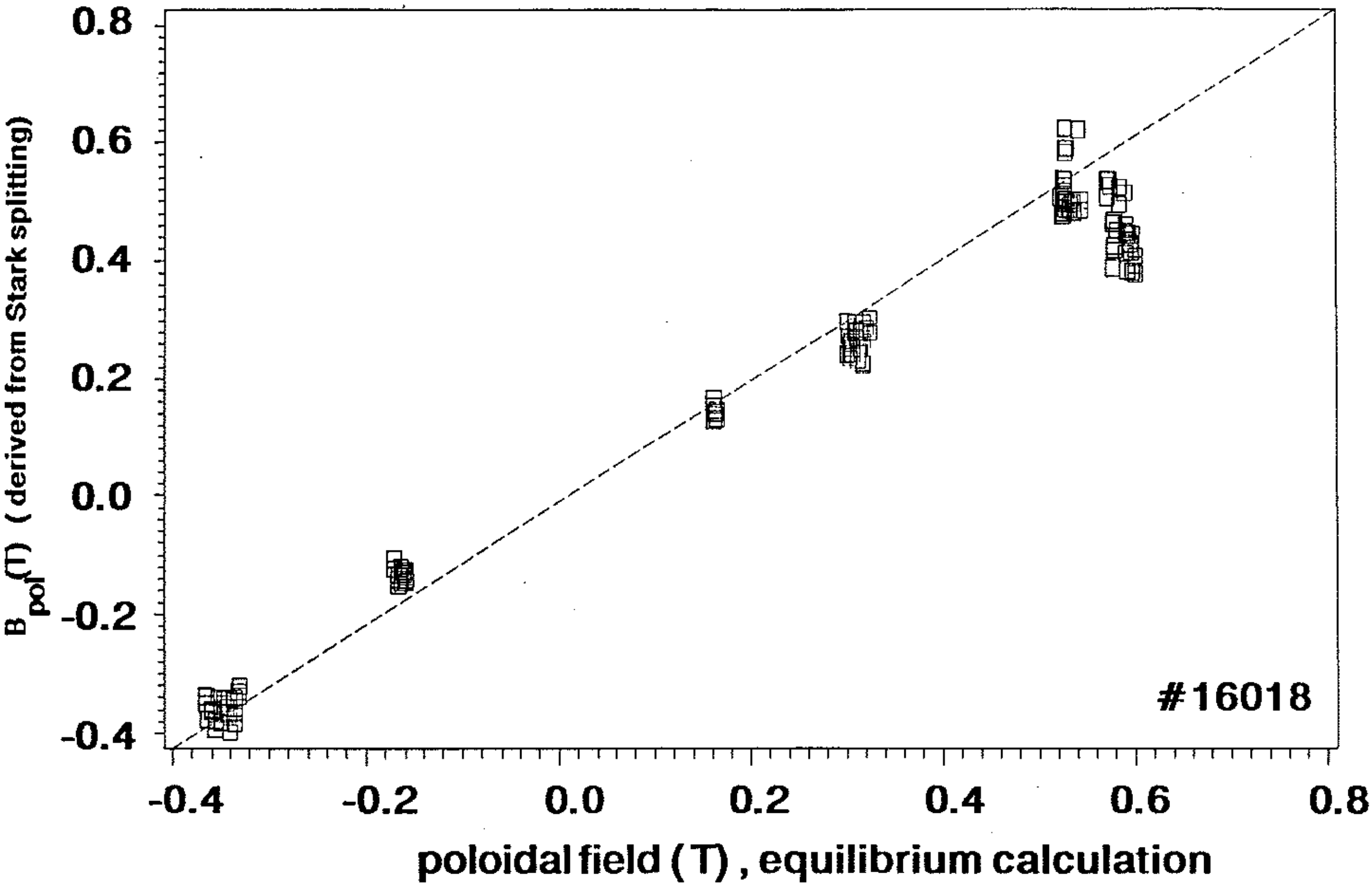

Fig.3 a)Active Balmer-Alpha CX spectrum from thermal plasma deuterons and Doppler-shifted impact spectrum from fast beam neutrals, with its motional Stark effect multiplet structure. The amplitudes of the unshifted edge D_{α} features are reduced in size for clarity. b) details of the multiplet structure, repeated for the half and third energy beam component. A special fit is applied which constrains the multiplet peaks to equi-separated distances. The statistical accuracy of the local Lorentz field $\mathbf{E} = \mathbf{v} \times \mathbf{B}$, deduced from the wavelength separation, is of the order 1% c) shows for the same pulse poloidal field values deduced from the Stark splitting at different time slices for 6 CXRS radii and a comparison to values calculated by the JET equilibrium code.

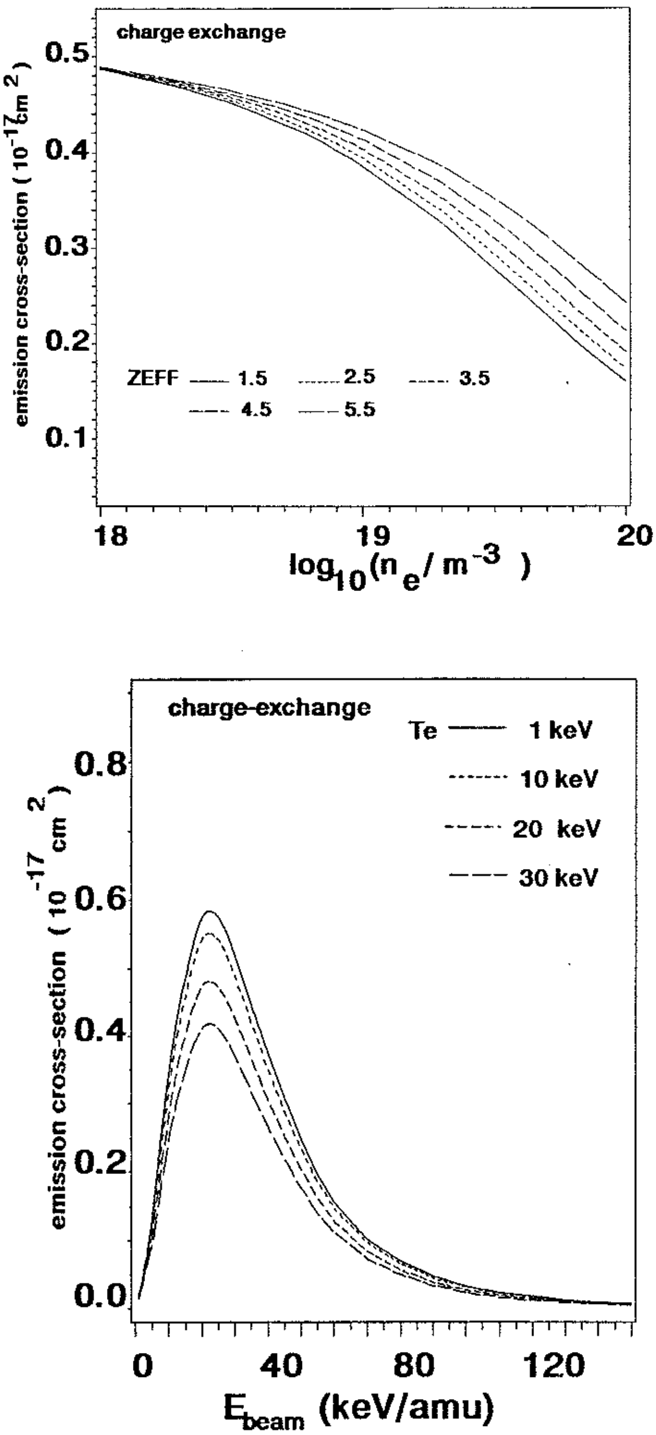

Fig.4 a)Balmer-Alpha effective charge excitation cross-section at 40 keV/amu for for different values of Z_{eff} as function of electron density the value of Z_{eff} refers to one impurity only) , b) CXRS excitation emission cross-section versus beam energy (Z_{eff}=3 and n_e= 1.6 $10^{19}m^{-3}$).

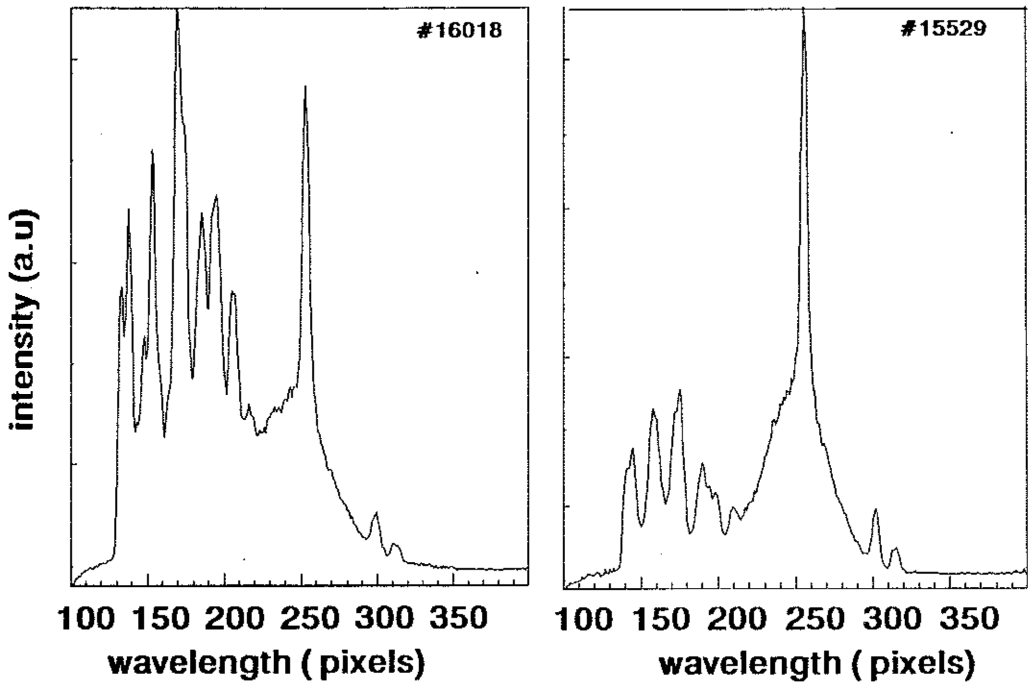

Fig.5 Two Balmer-alpha spectra for low and high Z_{eff} a)#16018, $<Z_{eff}>=3.3$, $n_e(0)=3.8\ 10^{19} m^{-3}$, b) #15529, $<Z_{eff}>=1.9$, $n_e=3.0\ 10^{19} m^{-3}$

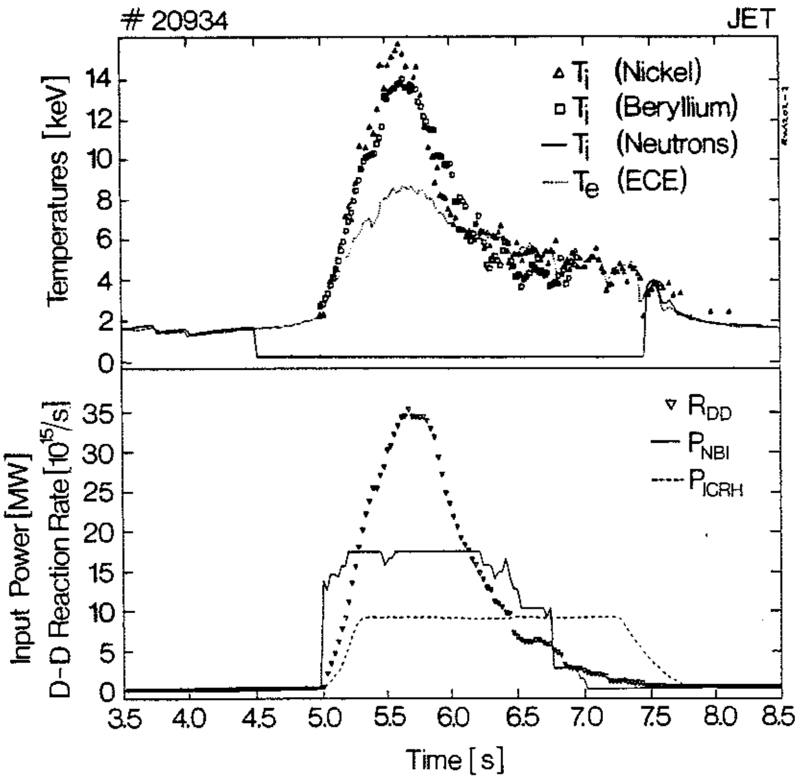

Fig.6 Central ion temperatures during ohmic and combined heating phases. During additional heating only $T_i(Ni^{26+})$ and $T_{i,CXR}(\ Be^{4+})$ are displayed, neutron production being no longer dominantly thermal.

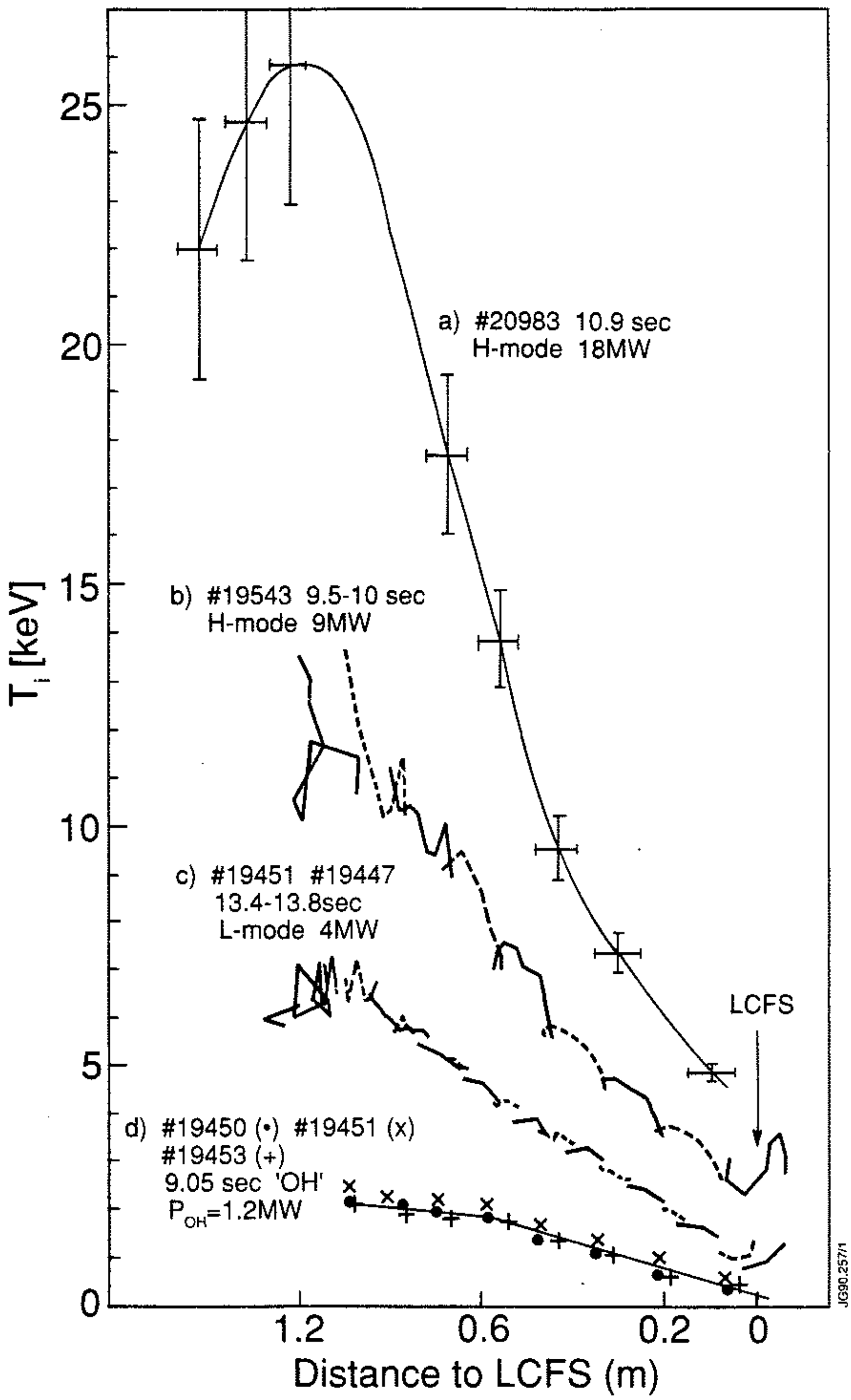

Fig 7 Ion temperature profiles in magnetic limiter plasmas from charge exchange measurements using the CVI n=8 to 7 transition at 5290.5 Å. The plasma was radially swept in cases b) and c) providing improved coverage of radii with a fixed fan of lines-of-sight. The abscissa is the distance to the last-closed-flux-surface (LCFS).

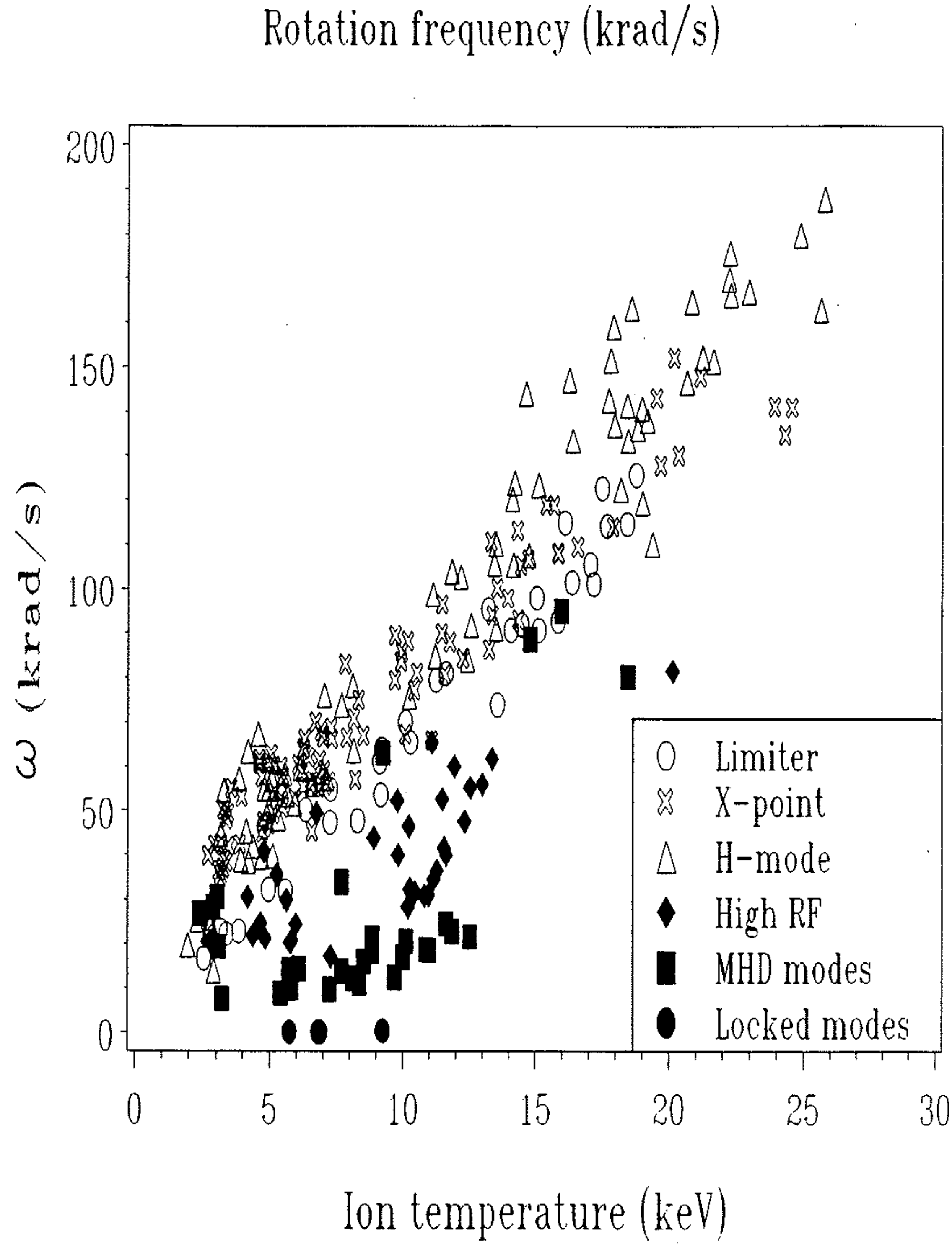

Fig.8 Survey of toroidal rotation frequency versus ion temperature in different plasma configuarations. The values of temperature and rotation velocities are not corrected for cross-section effects described in Fig. 2.

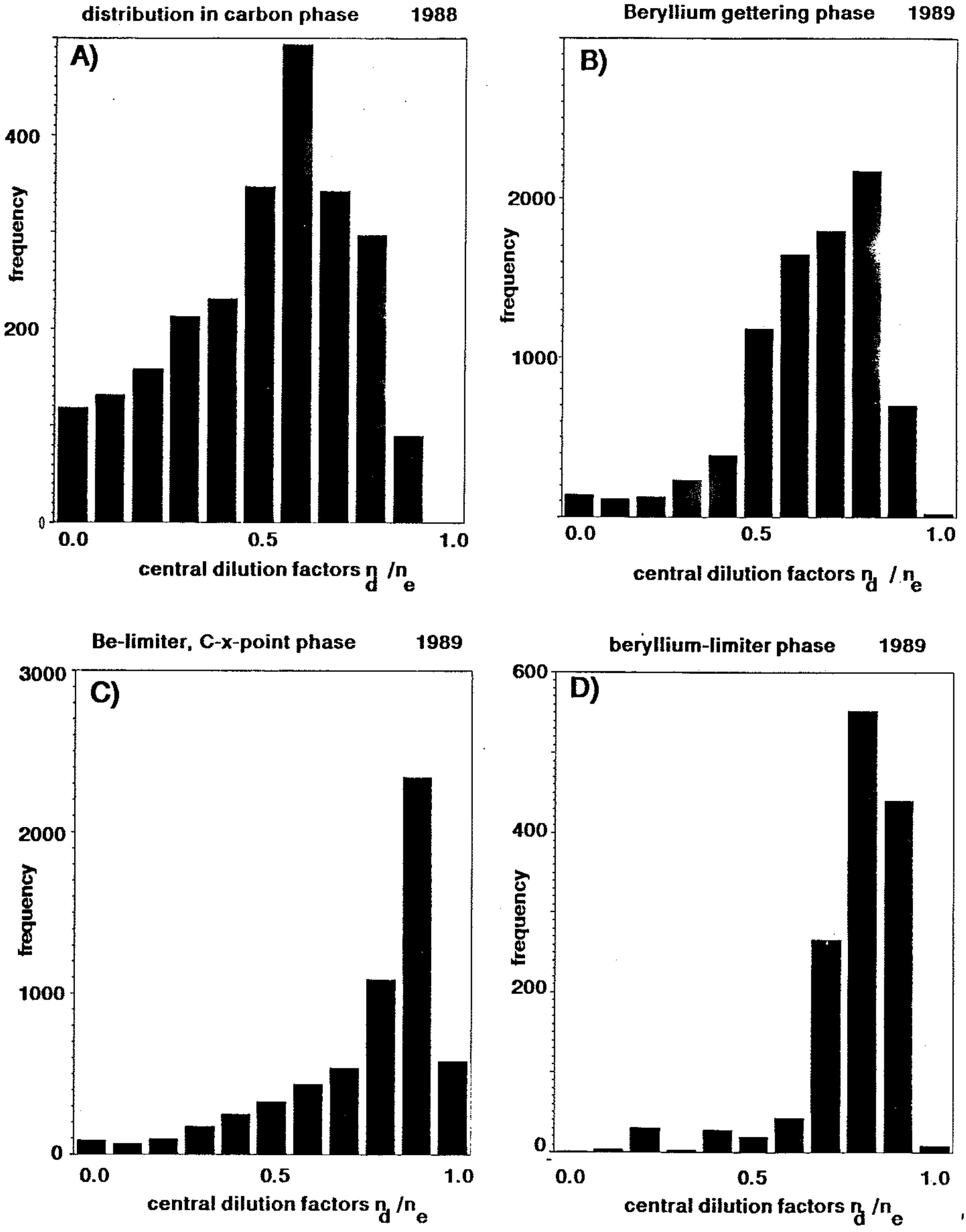

Fig. 9 Histograms of deuterium to electron density ratio A) All carbon vessel, all configurations B) Be gettering, all configurations C) & D) Be-belt-limiter installed C) X-point, Be gettering, C target plates D) Be-belt-limiter

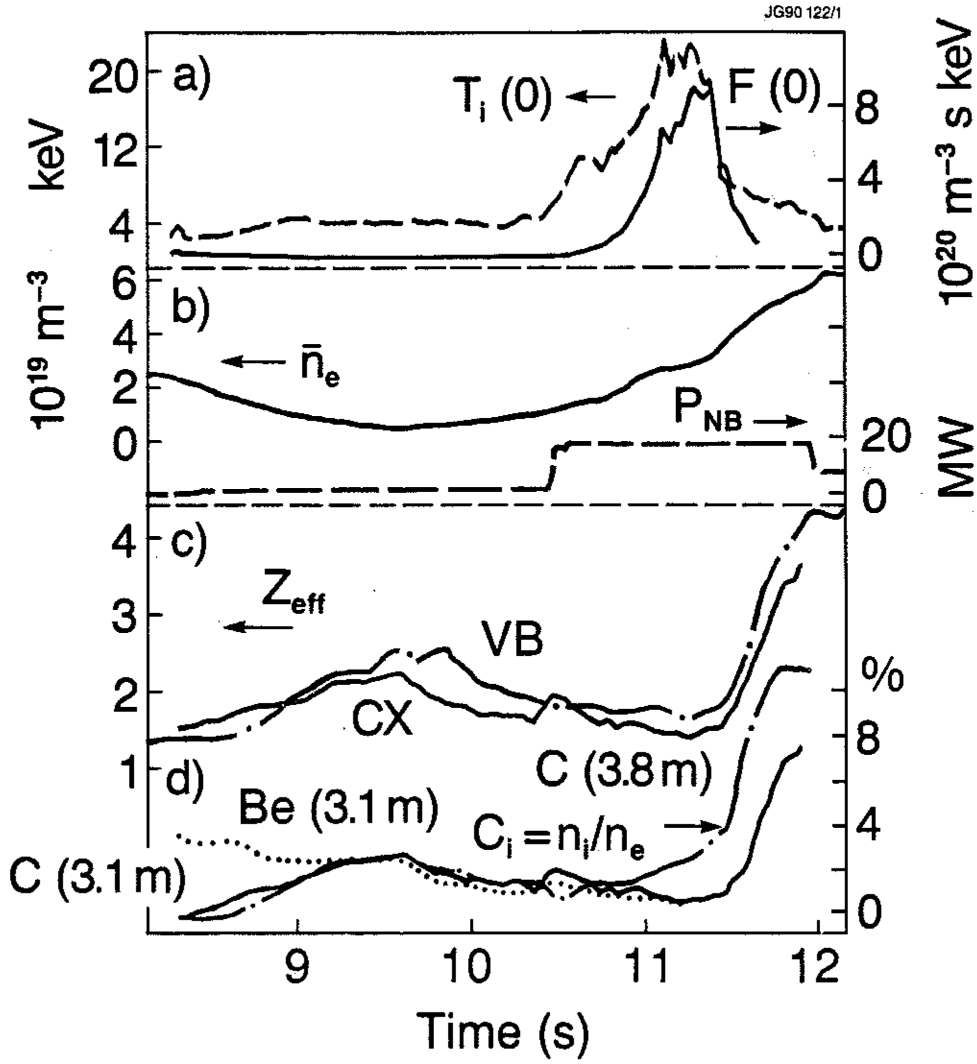

Fig.10 Impurity behaviour in a high-ion-temperature plasma in the double-null X-point configuration. The discharge was started on the Be belt-limiters. X-point formation was completed at 9.5 sec. An H-mode was established between 10.8 and 11.5 sec. B_T=2.8 T, I_P=4.1 MA (pulse # 20981).

a) Central ion temperature and fusion product from charge exchange spectroscopy b) Line electron density and neutral beam power c) Line averaged Z_{eff} from visible bremsstrahlung (VB) and central Z_{eff} from charge exchange (CX) d) Central Be (dots) and C (solid) concentrations (solid) and carbon concentration at 3.8 m (broken).

APPENDIX 1.

THE JET TEAM

JET Joint Undertaking, Abingdon, Oxon, OX14 3EA, U.K.

J. M. Adams[1], F. Alladio[4], H. Altmann, R. J. Anderson, G. Appruzzese, W. Bailey, B. Balet, D. V. Bartlett, L. R. Baylor[24], K. Behringer, A. C. Bell, P. Bertoldi, E. Bertolini, V. Bhatnagar, R. J. Bickerton, A. Boileau[3], T. Bonicelli, S. J. Booth, G. Bosia, M. Botman, D. Boyd[31], H. Brelen, H. Brinkschulte, M. Brusati, T. Budd, M. Bures, T. Businaro[4], H. Buttgereit, D. Cacaut, C. Caldwell-Nichols, D. J. Campbell, P. Card, J. Carwardine, G. Celentano, P. Chabert[27], C. D. Challis, A. Cheetham, J. Christiansen, C. Christodoulopoulos, P. Chuilon, R. Claesen, S. Clement[30], J. P. Coad, P. Colestock[6], S. Conroy[13], M. Cooke, S. Cooper, J. G. Cordey, W. Core, S. Corti, A. E. Costley, G. Cottrell, M. Cox[7], P. Cripwell[13], F. Crisanti[4], D. Cross, H. de Blank[16], J. de Haas[16], L. de Kock, E. Deksnis, G. B. Denne, G. Deschamps, G. Devillars, K. J. Dietz, J. Dobbing, S. E. Dorling, P. G. Doyle, D. F. Düchs, H. Duquenoy, A. Edwards, J. Ehrenberg[14], T. Elevant[12], W. Engelhardt, S. K. Erents[7], L. G. Eriksonn[5], M. Evrard[2], H. Falter, D. Flory, M. Forrest[7], C. Froger, K. Fullard, M. Gadeberg[11], A. Galetsas, R. Galvao[8], A. Gibson, R. D. Gill, A. Gondhalekar, C. Gordon, G. Gorini, C. Gormezano, N. A. Gottardi, C. Gowers, B. J. Green, F. S. Griph, M. Gryzinski[26], R. Haange, G. Hammett[6], W. Han[9], C. J. Hancock, P. J. Harbour, N. C. Hawkes[7], P. Haynes[7], T. Hellsten, J. L. Hemmerich, R. Hemsworth, R. F. Herzog, K. Hirsch[14], J. Hoekzema, W. A. Houlberg[24], J. How, M. Huart, A. Hubbard, T. P. Hughes[32], M. Hugon, M. Huguet, J. Jacquinot, O. N. Jarvis, T. C. Jernigan[24], E. Joffrin, E. M. Jones, L. P. D. F. Jones, T. T. C. Jones, J. Källne, A. Kaye, B. E. Keen, M. Keilhacker, G. J. Kelly, A. Khare[15], S. Knowlton, A. Konstantellos, M. Kovanen[21], P. Kupschus, P. Lallia, J. R. Last, L. Lauro-Taroni, M. Laux[33], K. Lawson[7], E. Lazzaro, M. Lennholm, X. Litaudon, P. Lomas, M. Lorentz-Gottardi[2], C. Lowry, G. Magyar, D. Maisonnier, M. Malacarne, V. Marchese, P. Massmann, L. McCarthy[28], G. McCracken[7], P. Mendonca, P. Meriguet, P. Micozzi[4], S.F. Mills, P. Millward, S. L. Milora[24], A. Moissonnier, P. L. Mondino, D. Moreau[17], P. Morgan, H. Morsi[14], G. Murphy, M. F. Nave, M. Newman, L. Nickesson, P. Nielsen, P. Noll, W. Obert, D. O'Brien, J. O'Rourke, M. G. Pacco-Düchs, M. Pain, S. Papastergiou, D. Pasini[20], M. Paume[27], N. Peacock[7], D. Pearson[13], F. Pegoraro, M. Pick, S. Pitcher[7], J. Plancoulaine, J-P. Poffé, F. Porcelli, R. Prentice, T. Raimondi, J. Ramette[17], J. M. Rax[27], C. Raymond, P-H. Rebut, J. Removille, F. Rimini, D. Robinson[7], A. Rolfe, R. T. Ross, L. Rossi, G. Rupprecht[14], R. Rushton, P. Rutter, H. C. Sack, G. Sadler, N. Salmon[13], H. Salzmann[14], A. Santagiustina, D. Schissel[25], P. H. Schild, M. Schmid, G. Schmidt[6], R. L. Shaw, A. Sibley, R. Simonini, J. Sips[16], P. Smeulders, J. Snipes, S. Sommers, L. Sonnerup, K. Sonnenberg, M. Stamp, P. Stangeby[19], D. Start, C. A. Steed, D. Stork, P. E. Stott, T. E. Stringer, D. Stubberfield, T. Sugie[18], D. Summers, H. Summers[20], J. Taboda-Duarte[22], J. Tagle[30], H. Tamnen, A. Tanga, A. Taroni, C. Tebaldi[23], A. Tesini, P. R. Thomas, E. Thompson, K. Thomsen[11], P. Trevalion, M. Tschudin, B. Tubbing, K. Uchino[29], E. Usselmann, H. van der Beken, M. von Hellermann, T. Wade, C. Walker, B. A. Wallander, M. Walravens, K. Walter, D. Ward, M. L. Watkins, J. Wesson, D. H. Wheeler, J. Wilks, U. Willen[12], D. Wilson, T. Winkel, C. Woodward, M. Wykes, I. D. Young, L. Zannelli, M. Zarnstorff[6], D. Zasche[14], J. W. Zwart.

PERMANENT ADDRESS

1. UKAEA, Harwell, Oxon. UK.
2. EUR-EB Association, LPP-ERM/KMS, B-1040 Brussels, Belgium.
3. Institute National des Récherches Scientifique, Quebec, Canada.
4. ENEA-CENTRO Di Frascati, I-00044 Frascati, Roma, Italy.
5. Chalmers University of Technology, Göteborg, Sweden.
6. Princeton Plasma Physics Laboratory, New Jersey, USA.
7. UKAEA Culham Laboratory, Abingdon, Oxon. UK.
8. Plasma Physics Laboratory, Space Research Institute, Sao José dos Campos, Brazil.
9. Institute of Mathematics, University of Oxford, UK.
10. CRPP/EPFL, 21 Avenue des Bains, CH-1007 Lausanne, Switzerland.
11. Risø National Laboratory, DK-4000 Roskilde, Denmark.
12. Swedish Energy Research Commission, S-10072 Stockholm, Sweden.
13. Imperial College of Science and Technology, University of London, UK.
14. Max Planck Institut für Plasmaphysik, D-8046 Garching bei München, FRG.
15. Institute for Plasma Research, Gandhinagar Bhat Gujat, India.
16. FOM Instituut voor Plasmafysica, 3430 Be Nieuwegein, The Netherlands.
17. Commissiariat à L'Energie Atomique, F-92260 Fontenay-aux-Roses, France.
18. JAERI, Tokai Research Establishment, Tokai-Mura, Naka-Gun, Japan.
19. Institute for Aerospace Studies, University of Toronto, Downsview, Ontario, Canada.
20. University of Strathclyde, Glasgow, G4 ONG, U.K.
21. Nuclear Engineering Laboratory, Lapeenranta University, Finland.
22. JNICT, Lisboa, Portugal.
23. Department of Mathematics, Univeristy of Bologna, Italy.
24. Oak Ridge National Laboratory, Oak Ridge, Tenn., USA.
25. G.A. Technologies, San Diego, California, USA.
26. Institute for Nuclear Studies, Swierk, Poland.
27. Commissiariat à l'Energie Atomique, Cadarache, France.
28. School of Physical Sciences, Flinders University of South Australia, South Australia SO42.
29. Kyushi University, Kasagu Fukuoka, Japan.
30. Centro de Investigaciones Energeticas Medioambientales y Techalogicas, Spain.
31. University of Maryland, College Park, Maryland, USA.
32. University of Essex, Colchester, UK.
33. Akademie de Wissenschaften, Berlin, DDR.

CR 88.49.1A